MODIFIED GRAVITY AND COSMOLOGY: An Update by the CANTATA Network

Emmanuel N. Saridakis[1,2,3], **Ruth Lazkoz**[4], **Vincenzo Salzano**[5], **Paulo Vargas Moniz**[6,7], **Salvatore Capozziello**[8,9,10], **Jose Beltrán Jiménez**[11], **Mariafelicia De Laurentis**[12,8,10], **Gonzalo J. Olmo**[13,14] **(Editors)**

Yashar Akrami[15,16], **Sebastian Bahamonde**[17,18], **Jose Luis Blázquez-Salcedo**[19], **Christian G. Böhmer**[18], **Camille Bonvin**[20], **Mariam Bouhmadi-López**[21,4], **Philippe Brax**[22], **Gianluca Calcagni**[23], **Roberto Casadio**[24,25], **Jose A. R. Cembranos**[19], **Álvaro de la Cruz-Dombriz**[26], **Anne-Christine Davis** [7], **Adrià Delhom**[13], **Eleonora Di Valentino**[27], **Konstantinos F. Dialektopoulos**[28], **Benjamin Elder**[29,30], **Jose María Ezquiaga**[31], **Noemi Frusciante**[32], **Remo Garattini**[33,34], **László Á. Gergely**[35], **Andrea Giusti**[36], **Lavinia Heisenberg**[37], **Manuel Hohmann**[17], **Damianos Iosifidis**[38], **Lavrentios Kazantzidis**[39], **Burkhard Kleihaus**[40], **Tomi S. Koivisto**[17,41,42,43], **Jutta Kunz**[40], **Francisco S. N. Lobo**[32], **Matteo Martinelli**[44,45], **Prado Martín-Moruno**[19], **José Pedro Mimoso**[32], **David F. Mota**[46], **Simone Peirone**[44], **Leandros Perivolaropoulos**[39], **Valeria Pettorino**[47], **Christian Pfeifer**[17], **Lorenzo Pizzuti**[48], **Diego Rubiera-Garcia**[19], **Jackson Levi Said**[49,50], **Mairi Sakellariadou**[51], **Ippocratis D. Saltas**[52], **Alessio Spurio Mancini**[53], **Nicoleta Voicu**[54], **Aneta Wojnar**[17] **(Section Contributors)**

Abstract

General Relativity and the ΛCDM framework are currently the standard lore and constitute the concordance paradigm. Nevertheless, long-standing open theoretical issues, as well as possible new observational ones arising from the explosive development of cosmology the last two decades, offer the motivation and lead a large amount of research to be devoted in constructing various extensions and modifications.

All extended theories and scenarios are first examined under the light of theoretical consistency, and then are applied to various geometrical backgrounds, such as the cosmological and the spherical symmetric ones. Their predictions at both the background and perturbation levels, and concerning cosmology at early, intermediate and late times, are then confronted with the huge amount of observational data that astrophysics and cosmology are able to offer recently. Theories, scenarios and models that successfully and efficiently pass the above steps are classified as viable and are candidates for the description of Nature.

This work is a Review of the recent developments in the fields of gravity and cosmology, presenting the state of the art, high-lighting the open problems, and outlining the directions of future research. Its realization was performed in the framework of the COST European Action “Cosmology and Astrophysics Network for Theoretical Advances and Training Actions”.

Contents

Introduction **11**

1 Cosmophysics of modified gravity **13**

2 General Relativity **26**

3 Foundations of Gravity – Modifications and Extensions **32**

3.1 Preliminaries 32
3.2 Matter Couplings 34
3.3 The Einstein-Hilbert Action – Linear Extensions 35
3.4 The Einstein-Hilbert Action – Nonlinear Extensions 38

Part I: Theories of Gravity **41**

4 Introduction to Part I **41**

5 A Flavour on $f(R)$ Theories: Theory and Observations **43**

5.1 Historia, Lux Veritatis 43
5.2 Scalar-Tensor Theories 45
5.2.1 Field Equations of Scalar-Tensor Gravity 45
5.2.2 Brans-Dicke Theory 46
5.3 Introduction to $f(R)$ Gravity 47
5.3.1 $f(R)$ Formalisms 48
5.3.2 $f(R)$ Gravity From a Scalar-Tensor Perspective 50
5.3.3 Viability 51
5.4 Background Cosmology in the Metric Formulation 56
5.5 Scalar Perturbations: the 1+3 Formalism 57
5.5.1 Fluid Sources 58
5.5.2 Geometry 59
5.5.3 Propagation and Constraint Equations 60
5.6 Geodesic Deviation in $f(R)$ Gravity 63
5.6.1 Formalism 63
5.6.2 Past-directed Null Geodesics and Area Distance in $f(R)$ Gravity 64
5.7 Gravitational Attractiveness in $f(R)$? 65
5.8 Conclusions 66

6 Horndeski/Galileon theories **68**
6.1 From Brans–Dicke to Horndeski . . . 68
6.2 Background Cosmology . . . 70
6.3 Cosmological Perturbations . . . 71
6.4 Gravitational Waves Constraints . . . 72

7 Massive Gravity and Bimetric Gravity **74**
7.1 Massive and Bimetric Gravity . . . 74
7.2 Cosmological Applications . . . 77

8 Gravity in Extra Dimensions **79**
8.1 Kaluza-Klein Model . . . 79
8.2 Large Extra Dimensions . . . 80
8.2.1 Brane Worlds . . . 80
8.2.2 Universal Extra Dimensions . . . 83
8.2.3 Mixed Models . . . 83

9 Non-local Gravity **85**
9.1 UV Nonlocal Gravity . . . 86
9.2 IR Nonlocal Gravity . . . 91

10 Metric-Affine Gravity **95**
10.1 Geometrical Objects: Torsion, Curvature and non-Metricity . . . 95
10.2 Geometrical Meaning of Torsion and Non-metricity . . . 97
10.2.1 Geometrical Meaning of Torsion . . . 97
10.2.2 Geometrical Meaning of Non-Metricity . . . 99
10.3 Identities of non-Riemannian Geometry . . . 100
10.3.1 The Sources of Metric-Affine Gravity . . . 101
10.4 Field Equations of Metric-Affine Gravity . . . 101
10.5 The Differential Form Formulation of Metric-Affine Gravity . . . 102
10.6 Conservation Laws and Hyperfluid Models . . . 102
10.6.1 Hyperfluids in Cosmology . . . 103

11 Geometric Foundations of Gravity **105**
11.1 Metric-affine geometry . . . 105
11.2 The Geometrical Trinity . . . 107
11.3 Purified Gravity . . . 109
11.3.1 Field Equations . . . 110
11.3.2 Energy and Entropy . . . 110
11.3.3 On Quantum Theory . . . 112
11.3.4 Matter Coupling . . . 113
11.4 Modified Gravity . . . 115

12 Palatini Theories of Gravity and Cosmology **118**
12.1 Smoothing out Cosmological Singularities . . . 119
12.2 Inflationary Models . . . 120
12.3 Background Evolution, Late-time Acceleration, and Observational Constraints . . . 122

13 Hybrid Metric-Palatini Gravity and Cosmology **125**
13.1 Hybrid Metric-Palatini Gravity: The General Formalism . . . 126
13.1.1 Action and Gravitational Field Equations . . . 126
13.1.2 Scalar-tensor Representation . . . 127
13.2 Hybrid-gravity Cosmology . . . 128
13.2.1 Background Expansion . . . 129
13.2.2 Cosmological Perturbations . . . 131
13.3 Discussions and Final Remarks . . . 134

14 Teleparallel Gravity: Foundations and Cosmology **135**
14.1 Foundations of Teleparallel Gravity . . . 135
14.1.1 Teleparallel Geometry . . . 135
14.1.2 Translation Gauge Theory . . . 136
14.1.3 Local Lorentz Invariance . . . 138
14.1.4 Matter Coupling . . . 139
14.1.5 Teleparallel Equivalent of General Relativity (TEGR) . . . 139
14.2 Teleparallel Gravity Extensions . . . 141
14.2.1 $f(\mathbb{T})$ Gravity . . . 141
14.2.2 New General Relativity and Extensions . . . 142
14.2.3 Higher-order Derivatives, $f(\mathbb{T}, B, T_{\mathcal{G}}, B_{\mathcal{G}})$ . . . 143
14.2.4 Teleparallel Non-local Theories . . . 144
14.2.5 Horndeski Analog and Subclasses . . . 145
14.2.6 Teleparallel Dark Energy Models . . . 146
14.3 Phenomenology of Teleparallel Gravity . . . 146
14.3.1 $f(\mathbb{T})$ Cosmology and the Power-law Model . . . 148
14.3.2 Cosmography in $f(\mathbb{T})$ Gravity . . . 149
14.3.3 The Growth Factor . . . 150
14.3.4 The H_0 Tension Problem . . . 152
14.3.5 Inflation in Teleparallel Theories of Gravity . . . 155
14.3.6 Dynamical System in Cosmology for Teleparallel Theories of Gravity . . . 156
14.3.7 Noether Symmetry Approach in Teleparallel Theories of Gravity . . . 160
14.3.8 Bounce Solutions in Modified Teleparallel Cosmology . . . 162
14.4 What Can Teleparallel Theories Have to Offer? What Are the Open Problems in Teleparallel Theories? . . . 164

15 Finsler Gravity **168**
15.1 Physical Motivations . . . 168
15.1.1 Finsler Geometry in Physics . . . 168
15.1.2 Finsler Gravity . . . 169
15.1.3 Finsler Cosmology . . . 170
15.2 Definition of Finsler Spacetimes . . . 170
15.2.1 Positive Definite Finsler Manifolds . . . 171
15.2.2 Finsler Spacetime . . . 171
15.2.3 Geodesics, Geodesic Deviation and Curvature Scalar . . . 173
15.3 Finslerian Scalars as Physical Fields . . . 175
15.4 Gravitational Dynamics . . . 176
15.4.1 The kinetic Gas Action on the Tangent Bundle . . . 177
15.4.2 The Finsler Gravity Action . . . 178
15.4.3 Kinetic Gases as Physical Sources for Finsler Gravity . . . 178

16 Gravity's Rainbow **180**
16.1 The Cosmological Constant as a Sturm-Liouville Eigenvalue Problem 181
16.2 From Quantum Mechanics to Quantum Field Theory 183
16.2.1 The Wheeler-DeWitt Equation Distorted by Gravity's Rainbow 185
16.3 Correspondence of Gravity's Rainbow With Hořava-Lifshitz Gravity 186

17 Quantum Cosmology in Modified Theories of Gravity **189**
17.1 Quantum Cosmology in a Metric Theory 189
17.2 Quantum Cosmology in a Palatini Theory 190

Part II: Testing Relativistic Effects **192**

18 Introduction to Part II **192**

19 Laboratory Constraints **194**
19.1 Chameleons in Laboratory Vacuums 195
19.2 Atom Interferometry 195
19.3 Eöt-Wash 197
19.4 Casimir 197
19.5 Neutron, Atomic and Electron Dipole Moment Tests 198
19.6 The Symmetron 198
19.7 Conclusions 199

20 Screening Mechanisms **200**
20.1 Screening 200
20.2 Laboratory Experiments and Quantum Effects 202
20.3 Other Screening Effects 203

21 Small-scale effects associated to non-metricity and torsion **204**
21.1 Small-scale Effects and Gravity 204
21.2 Small-scale Effects Associated to Non-metricity 205
21.2.1 Small-scale Effects in $f(\mathcal{R})$ Theories 207
21.2.2 Small-scale Effects in Generic RBGs 209
21.3 Small-scale Effects Associated with Torsion 210
21.4 Outlook 214

22 Stars as Tests of Modified Gravity **215**
22.1 Modified Tolman-Oppenheimer-Volkoff Equations 215
22.2 Modified Lane-Emden Equation 217

23 Compact Objects in General Relativity and Beyond **219**
23.1 Neutron Stars 219
23.1.1 Neutron Stars in General Relativity 219
23.1.2 Neutron Stars in Generalized Theories of Gravity 224
23.2 Black Holes 228
23.2.1 Black Holes in General Relativity 228
23.2.2 Black Holes in Generalized Theories of Gravity 229
23.3 Conclusions 232

24 Parametrized Post-Newtonian Formalism **233**
24.1 Historical remarks . . . 233
24.2 Parametrized post-Newtonian Formalism . . . 234
24.3 Comparison to Observations . . . 235
24.4 Extensions and Modifications . . . 236
24.4.1 Invariant density formulation . . . 236
24.4.2 Broken Diffeomorphism Invariance . . . 237
24.4.3 Yukawa-type Couplings . . . 237
24.4.4 Higher Derivative Orders . . . 237
24.4.5 Parity-violating Terms . . . 237
24.4.6 Screening Mechanisms . . . 238
24.4.7 Cosmological Background Evolution . . . 238
24.4.8 Multiple Metrics . . . 238
24.4.9 Tetrad Formulation . . . 238
24.4.10 Gauge-invariant Approach . . . 239
24.5 Post-Newtonian Limit of Particular Theories . . . 239
24.5.1 Scalar-tensor and $f(R)$ Theories . . . 239
24.5.2 Multi-scalar-tensor Theories . . . 240
24.5.3 Horndeski Gravity . . . 240
24.5.4 Bimetric and Multimetric Gravity . . . 240
24.5.5 Teleparallel Gravity . . . 241

25 Gravitational Waves **242**
25.1 Tests of General Relativity . . . 242
25.2 Modified Gravity . . . 245
25.3 Quantum Gravity . . . 246

26 Gravitational Lensing **248**
26.1 Deflection of Light in Schwarzschild Geometry . . . 248
26.2 Deflection of Light by Spherically Symmetric, Static Tidal Charged Brane Black Holes . . . 250
26.3 The Lens Equation . . . 252
26.4 Image Positions . . . 253
26.5 Magnification Ratios . . . 254
26.6 Strong Lensing by Spherically Symmetric, Static Tidal Charged Black Holes . . . 254
26.7 Gravitational Lensing by Other Spherically Symmetric, Static Brane Black Holes 255
26.8 Gravitational Lensing in Hořava-Lifshitz Gravity . . . 256
26.9 Gravitational Lensing in $f(R)$ Gravity . . . 257
26.10 Gravitational Lensing in Scalar-Tensor Theories . . . 258
26.11 Gravitational Lensing in Teleparallel Gravity . . . 258
26.12 Gravitational Lensing, Galaxies and Cosmology . . . 259
26.13 Concluding Remarks . . . 259

27 Classicalizing Gravity **261**
27.1 Semiclassical Gravity and Localized Quantum States . . . 261
27.2 Corpuscular Gravity . . . 262
27.3 Gravitational Collapse . . . 264
27.4 Bootstrapping Newton . . . 265
27.5 Quantum Compositeness of Gravity at Cosmological Scales . . . 267
27.6 Outlook . . . 269

Part III: Cosmology and Observational Discriminators **270**

28 Introduction to Part III **270**

29 Phenomenological Tests of Gravity on Cosmological Scales **272**
29.1 Cosmological Tests of Gravity 272
29.1.1 Large Scales and the Linear Regime: Phenomenological Departures from GR 273
29.1.2 Cosmological Observables and Phenomenological Constraints 275
29.1.3 Einstein-Boltzmann Codes: from Theoretical Predictions to Data Analysis 279
29.1.4 Small Scales and Nonlinearities 280
29.2 Existing Constraints and Tensions 281
29.3 Upcoming Surveys and the Road Ahead 285

30 Relativistic Effects **288**
30.1 Number Counts 288
30.2 Correlation Function 289
30.2.1 Estimators 289
30.2.2 Even and Odd Multipoles 290
30.3 Test of the Equivalence Principle 292
30.4 Conclusions 296

31 Cosmological Constraints From the Effective Field Theory of Dark Energy **298**
31.1 The Effective Field Theory for Dark Energy in a Nutshell 298
31.2 Einstein Boltzmann Codes 299
31.3 Cosmological Constraints on Horndeski and GLPV Models 301
31.4 Astrophysical Constraints 304

32 The H_0 Tensions to Discriminate Among Concurring Models **307**
32.1 The Effective Number of Relativistic Degrees of Freedom 309
32.2 Dark Energy Equation of State 310
32.3 Multi-parameters Extension 310
32.4 Early Dark Energy 311
32.5 Interacting Dark Energy 312
32.6 Modified Gravity 312
32.7 More specific models 313
32.8 Requirements: Hubble Hunter's Guide 316
32.9 Standard Sirens 316

33 σ_8 Tension. Is Gravity Getting Weaker at Low z? Observational Evidence and Theoretical Implications **318**
33.1 The $f\sigma_8$ Tension and Modified Gravity. 326
33.1.1 Observational Evidence 326
33.1.2 Theoretical Implications 329
33.2 Evolving G_{eff} and the Pantheon SNeIa Dataset 332
33.3 Constraints on Evolving G_{eff} from Low l CMB Spectrum and the ISW Effect. . 335
33.4 Conclusions 336

34 Testing Gravity with Standard Sirens: Challenges and Opportunities 339
34.1 Gravitational Wave Propagation Beyond General Relativity . . . 339
34.2 Standard Sirens . . . 340
34.3 The Speed of GWs . . . 341
34.3.1 Constraints After GW170817 . . . 342
34.4 GW Luminosity Distance . . . 344
34.5 GW Oscillations . . . 346
34.6 Future Prospects . . . 347
34.6.1 Theoretical Challenges . . . 348
34.6.2 Observational Opportunities . . . 349

35 Testing the Dark Universe with Cosmic Shear 351
35.1 2D, Tomographic and 3D Weak Lensing . . . 351
35.2 Current Data and Forecasts on Horndeski Gravity . . . 354
35.3 Higher-order Statistics and Lensing Peak Counts . . . 357
35.4 Machine Learning and the Dark Universe . . . 357

36 Galaxy Clusters and Modified Gravity 360
36.1 What Makes Galaxy Clusters Interesting for Testing Gravity? . . . 360
36.2 Consistency Conditions Based on the Mass Profiles of Galaxy Clusters . . . 360
36.2.1 Generalities . . . 360
36.2.2 Probes Based on Mass Profiles from Galaxy Kinematics and Lensing . . . 361
36.2.3 Probes Based on Thermal and Lensing Mass Profiles . . . 363
36.3 A Brief Discussion on Systematics . . . 364
36.4 Future Outlook . . . 367

37 Probing Screening Modified Gravity with Non-linear Structure Formation 368
37.1 Theoretical Models . . . 369
37.1.1 Chameleon-$f(R)$ Gravity . . . 370
37.1.2 Symmetron . . . 370
37.2 Efficiency of Screening Mechanisms . . . 371
37.2.1 Solar System Constraints . . . 371
37.2.2 Simulations . . . 372
37.2.3 Results . . . 373
37.3 Distribution of Fifth Force in Dark Matter Haloes . . . 374
37.4 The Matter and the Velocity Power Spectra . . . 374
37.5 The Dynamical and Lensing Masses . . . 375
37.6 Thermal Versus Lensing Mass Measurements . . . 376
37.6.1 Including the Non-thermal Pressure Component . . . 377
37.7 Modelling Void Abundance in Modified Gravity . . . 379
37.7.1 Linear Power Spectrum . . . 379
37.7.2 Spherical Collapse . . . 381
37.7.3 Void Abundance Function . . . 382
37.7.4 Voids from Simulations . . . 385
37.7.5 Results . . . 386
37.8 Conclusions and Perspectives . . . 389

Conclusions **391**

38 The End of the Beginning **391**

Bibliography **401**

Index **541**

Preface

The dawn of the 21st century came with very positive prospects for gravity, cosmology and astrophysics. Technological progress made it possible for cosmology to enter to its adulthood and become a precision science, both for its own shake as well as for being the laboratory of gravity, which can now be accurately tested and investigated in scales different than the earth ones. As a result, the opinion that cosmology is one of the main directions that will lead to progress in physics in the near future, is now well established.

"Cosmology and Astrophysics Network for Theoretical Advances and Training Actions" (CANTATA) is a COST European Action established in 2015 in order to contribute to the front of research in the fields of gravity, cosmology and astrophysics. It involves Institutions from 26 European countries, as well as from 5 countries abroad. CANTATA Collaboration has a variety of interests, which include: i) the classification and definition of theoretical and phenomenological aspects of gravitational interaction that cannot be enclosed in the standard lore scheme but might be considered as signs of alternative theories of gravity, ii) the confrontation of the theoretical predictions with observations at both the background and the perturbation levels, iii) the production of numerical codes to simulate astrophysical and cosmological phenomena, iv) the construction of self-consistent models at various scales and the investigation of the features capable of confirming or ruling out an effective theory of gravity, v) the study of how extended and modified theories of gravity emerge from quantum field theory and how mechanisms produced by the latter may explain cosmological dynamics. This Review presents the recent developments in the above fields.

Emmanuel N. Saridakis
Ruth Lazkoz
Vincenzo Salzano
Paulo Vargas Moniz
Salvatore Capozziello
Jose Beltrán Jiménez
Mariafelicia De Laurentis
Gonzalo J. Olmo

Conventions

Greek small letters α, μ, ν,...	space-time coordinates indices
Latin small letters i, j, k...	space coordinates indices
Latin capital indices A, B,...	tangent space indices (only in chapters 8 and 9 D-dimensional coordinate indices)
$g_{\mu\nu}$	metric tensor
(-+++)	metric signature
${\Gamma^\mu}_{\nu\rho}$	Levi-Civita connection
${R^\mu}_{\nu\alpha\beta} = \partial_\alpha {\Gamma^\mu}_{\nu\beta} - \partial_\beta {\Gamma^\mu}_{\nu\alpha} + {\Gamma^\mu}_{\sigma\alpha}{\Gamma^\sigma}_{\nu\beta} - {\Gamma^\mu}_{\sigma\beta}{\Gamma^\sigma}_{\nu\alpha}$	Riemann curvature tensor
$R_{\mu\nu} = {R^\alpha}_{\mu\alpha\nu}$	Ricci tensor
$R = {R^\alpha}_\alpha$	Ricci scalar
$G_{\mu\nu} = R_{\mu\nu} - \frac{1}{2}g_{\mu\nu}R$	Einstein tensor
∇_μ	covariant derivative
$\Box \equiv g^{\mu\nu}\nabla_\mu\nabla_\nu$	d'Alembertian operator
$2X_{[\alpha\beta]} = X_{\alpha\beta} - X_{\beta\alpha}$	anti-symmetricity
$2X_{(\alpha\beta)} = X_{\alpha\beta} + X_{\beta\alpha}$	symmetricity
$ds^2 = -dt^2 + a^2(t)\left[\frac{dr^2}{1-kr^2} + r^2\left(d\theta^2 + \sin^2\theta d\phi^2\right)\right]$	4-dimensional Friedmann-Lemaître- Robertson-Walker (FLRW) line-element
$\tau = \int dt/a(t)$	conformal time
$\dot{} \equiv \frac{d}{dt}$	cosmic time derivative
$' \equiv \frac{d}{d\tau}$	conformal time derivative
$ds^2_{(3)} = \gamma_{ij}dx^i dx^j = \frac{dr^2}{1-kr^2} + r^2 d\theta^2 + r^2\sin^2\theta d\phi^2$	maximally symmetric 3-dimensional space-like hyper-surfaces metric
$\vec{\nabla}_i$	grad operator on the 3-dimensional space-like hyper-surfaces
$\Delta \equiv \gamma^{ij}\vec{\nabla}_i\vec{\nabla}_j$	Laplacian operator
$ds^2 = -(1+2\Psi)dt^2 + a^2(t)(1-2\Phi)\gamma_{ij}dx^i dx^j$	Newtonian gauge scalar metric perturbations
$T^{\mu\nu} = \frac{2}{\sqrt{-g}}\frac{\delta\mathcal{L}_m}{\delta g_{\mu\nu}}$	energy-momentum tensor of the Lagrangian density $\mathcal{L}$
$\kappa^2 \equiv 8\pi G_N \equiv M_{Pl}^{-2}$	gravitational constant
$\hbar = c = k_B = 1$	natural units

List of notational conventions used in this manuscript, unless otherwise stated.

$\hat{\Gamma}^{\alpha}_{\mu\nu}$	general affine connection
$\breve{\Gamma}^{\alpha}_{\mu\nu}$	Palatini connection
$\overset{\bullet}{\Gamma}{}^{\alpha}_{\mu\nu}$	teleparallel affine (Weitzenböck) connection
$\overset{\diamond}{\Gamma}{}^{\alpha}_{\mu\nu}$	symmetric teleparallel connection
$\overline{\Gamma}^{\alpha}_{\mu\nu}$	Chern-Rund linear connection
$\bar{\bar{\Gamma}}{}^{\mu}{}_{\nu}$	canonical nonlinear connection
$\bigcirc$	arbitrary object wrt the Levi-Civita connection
$\hat{\bigcirc}$	arbitrary object wrt the metric affine connection
$\breve{\bigcirc}$	arbitrary object wrt the Palatini connection
$\overset{\bullet}{\bigcirc}$	arbitrary object wrt the Weitzenböck connection
$\overset{\diamond}{\bigcirc}$	arbitrary object wrt the symmetric teleparallel connection
$\overline{\bigcirc}$	arbitrary object wrt the Chern-Rund linear connection
$\bar{\bar{\bigcirc}}$	arbitrary object wrt the canonical nonlinear connection
$\omega^{A}{}_{B\mu}$	spin connection
D_{μ}	Fock-Ivanenko derivative
$T^{\mu}{}_{\nu\rho}$	torsion tensor
$Q_{\alpha\mu\nu} = \nabla_{\alpha} g_{\mu\nu}$	non-metricity tensor
$T_{\mu} = T^{\nu}{}_{\nu\mu}$	torsion vector
$\hat{\tilde{\hat{R}}}_{\alpha\beta} := \hat{R}^{\mu}{}_{\mu\alpha\beta}$	homothetic curvature
$\hat{\tilde{\hat{\mathcal{R}}}}{}^{\lambda}{}_{\kappa} := \hat{R}^{\lambda}{}_{\mu\nu\kappa} g^{\mu\nu}$	co-Ricci tensor
$\mathcal{R} \equiv g^{\mu\nu}\mathcal{R}_{\mu\nu} \equiv g^{\mu\nu}\left(\breve{\Gamma}^{\alpha}_{\mu\nu,\alpha} - \breve{\Gamma}^{\alpha}_{\mu\alpha,\nu} + \breve{\Gamma}^{\alpha}_{\alpha\lambda}\breve{\Gamma}^{\lambda}_{\mu\nu} - \breve{\Gamma}^{\alpha}_{\mu\lambda}\breve{\Gamma}^{\lambda}_{\alpha\nu}\right)$	Palatini curvature
$e^{A}{}_{\mu}$	tetrad (vielbein, coframe)
$e_{A}{}^{\mu}$	frame dual to $e^{A}{}_{\mu}$
$K^{\mu}{}_{\nu\rho}$	contortion tensor
$L^{\mu}{}_{\nu\rho}$	distortion tensor
$S_{\mu}{}^{\nu\rho}$	superpotential
$\mathbb{T}$	torsion scalar
$\mathbb{Q}$	non-metricity scalar
$\epsilon_{\mu\alpha\beta\gamma}$	4-dimensional totally antisymmetric Levi-Civita tensor

(cont.) List of notational conventions used in this manuscript, unless otherwise stated.

35. Testing the Dark Universe with Cosmic Shear

Valeria Pettorino, Alessio Spurio Mancini

Although a cosmological constant framework is still in agreement with current data, several other cosmological models in which gravity is modified are also still viable. There are several approaches that one can adopt in order to distinguish ΛCDM from modified gravity models. One can try to: a) use or combine different probes, b) get more data, c) improve the analysis to extract more information from the available data. Below we focus on weak lensing, its different approaches and the impact of statistics we use on constraining or distinguishing cosmological models.

Weak lensing describes, in particular, small distortions in the observed image of galaxy shapes, induced by the presence of massive structures along the line of sight. Weak lensing can be typically described in terms of shear and convergence fields, quantifying anisotropic and isotropic distortions respectively. Convergence can be derived from shear, up to a constant, and both depend on the angular position θ on the sky. Given a convergence map $\kappa(\theta)$ for a particular realisation of a model, one can also compute the aperture mass map [2161, 2162] by applying a filter (see, for example, [2163] for a review of different filters adopted in literature).

In 35.1 we will recall different weak lensing methodologies; in 35.2 we will describe how well we can use current and future probes (in particular including cross-correlations or combining with galaxy clustering) to test modified gravity models; in 35.3 we recall how higher order statistics, and in particular peak counts, can help in breaking degeneracies between parameters; finally in 35.4 we illustrate recent results using machine learning techniques to improve the discrimination efficiency between ΛCDM and alternative theories in which gravity is modified with respect to General Relativity.

35.1 2D, Tomographic and 3D Weak Lensing

Here we provide a mathematical description of cosmic shear in a general modified gravity context, similar to the one presented in [2164]. We focus on two different formalisms commonly used to study the evolution in redshift of the lensing effect, so-called ‘tomography’ and ‘3D cosmic shear’. We assume spatial flatness throughout, and consider scalar linear perturbations on a Friedmann-Robertson-Walker metric, such that the line element in Newtonian gauge can be written as

$$ds^2 = -\,(1 + 2\Psi)\,dt^2 + a^2(t)\,(1 - 2\Phi)\,d\mathbf{x}^2, \tag{35.1}$$

with the scale factor $a(t)$ and the Bardeen potentials Ψ and Φ. In General Relativity $\Psi = \Phi$ in absence of anisotropic stress, but this is in general not true in a modified gravity theory. Poisson’s equation links one of the Bardeen potentials to the overdensity field $\delta(k, \chi)$,

$$\Psi(k, \chi) = -\frac{3}{2} \frac{\Omega_m}{(k\chi_H)^2} \frac{\delta(k, \chi)}{a(\chi)} \mu(k, a(\chi)), \tag{35.2}$$

with the Hubble radius $\chi_H \equiv 1/H_0$ and the function $\mu(k, a(\chi))$ parameterising variations from General Relativity, its value being 1 in standard gravity. We also define

$$\eta(k, a(\chi)) \equiv \frac{\Psi(k, a(\chi))}{\Phi(k, a(\chi))}, \tag{35.3}$$

as the ratio of the Bardeen potentials, again identically equal to 1 in General Relativity in absence of anisotropic stress. Other choices (such as Σ, defined in terms of the lensing potential $\Psi + \Phi$), of such two functions of time and scale are also possible, and may be more or less convenient; see [2165] or [2166] for a review.

A quantitative description of cosmic shear starts with the definition of the lensing potential

$$\Psi(\chi, \hat{\mathbf{n}}) = \int_0^{\chi} d\chi' \, \frac{\chi - \chi'}{\chi\chi'} \, [\Psi(\chi, \hat{\mathbf{n}}) + \Phi(\chi, \hat{\mathbf{n}})], \tag{35.4}$$

as a weighted projection of the sum of the Bardeen potentials along the line of sight. In Eq. 35.4, χ is the comoving distance and the normalised vector $\hat{\mathbf{n}}$ selects a direction in the sky. From its definition in Eq. 35.4 we notice that the lensing potential is sensitive to the growth of perturbations of the gravitational potentials, as well as to the geometry of the Universe through the weighting factor $\frac{\chi-\chi'}{\chi\chi'}$. We will assume that the integration in Eq. 35.4 is carried out along the unperturbed light path, following the Born approximation. The lensing observables, i.e., convergence and shear, are derived from the lensing potential through linear relations, so that these three fields share the same statistical properties. Hence, cosmic shear is sensitive to structure growth and the geometry of the Universe.

The sensitivity of cosmic shear to the growth of structure is particularly important in studies of cosmic acceleration, as different dark energy and modified gravity models are endowed with different predictions for structure growth. As a consequence, it is crucial to include redshift information in a cosmic shear analysis, so that the effect of dark energy on structure growth can be studied in its evolution with redshift. A two-dimensional analysis (like the one carried out in [2167], for example) can achieve this goal only to a limited extent, as it projects quantities along the line of sight; this implies loss of redshift information, due to the mixing of spatial scales and to the reduced sensitivity to those parameters that, entering the model in a nonlinear way, may produce different effects on the lensing signal at different redshifts [2168].

To overcome the limitations of a purely two-dimensional analysis, a formalism was first introduced in [2169], which assigns galaxies to different redshift bins according to their estimated (photometric) redshift, and calculates correlations of the lensing signal through redshift bins. This approach is commonly known as *tomography* and is the most common methodology to analyse a cosmic shear survey (as used, e.g., in [2170]). The integration along the line of sight that characterises a two-dimensional analysis is here reduced to the width of the redshift bin; the correlation among different redshift bins provides information on the evolution in redshift of the lensing signal. Defining the matter power spectrum $P_\delta(k)$ as

$$\langle \delta(\mathbf{k}, z) \delta(\mathbf{k}', z) \rangle = (2\pi)^3 P_\delta(k, z) \delta^D(\mathbf{k} - \mathbf{k}'), \tag{35.5}$$

and making use of the Limber approximation [1587, 2171, 2172], one can write down the flat-sky tomographic convergence power spectrum between tomographic bins i and j as

$$C_{ij}^{\kappa}(\ell) = \int \frac{d\chi}{\chi^2} \, W_i(\ell/\chi, \chi) \, W_j(\ell/\chi, \chi) \, P_\delta(\ell/\chi, \chi), \tag{35.6}$$

where the lensing efficiency function $W_i(\ell/\chi, \chi)$ is defined as

$$W_i(\ell/\chi, \chi) = \frac{3\Omega_m}{4\chi_H^2} \int_\chi^\infty d\chi' \, \frac{dz}{d\chi'} \, \frac{n_i(z(\chi'))}{a(\chi')} \left(\frac{\chi - \chi'}{\chi\chi'}\right) \left[1 + \frac{1}{\eta(\ell/\chi, \chi')}\right] \mu(\ell/\chi, \chi'), \qquad (35.7)$$

with $n_i(z(\chi))$ the distribution of sources in the i-th bin, normalized to one, $\int d\chi \, n_i(z(\chi)) = 1$. Clearly, this approach still remains an approximation to a purely 3-dimensional treatment of the cosmic shear field, as it is still characterised by an averaging in redshift, which produces loss of information.

An alternative formalism, commonly known as *3D cosmic shear*, makes use of a spherical Fourier-Bessel decomposition of the cosmic shear field, to include all of the redshift information in the analysis. First introduced in [2173] and subsequently refined in [2174–2176], this method has so far been applied to real data only in [2177]. A code comparison between available codes and numerical challenges have been discussed in [2178]. 3D cosmic shear is based on a decomposition of the cosmic shear field in a suitable basis of functions, given by a combination of spin-2 spherical harmonics ${}_2Y_{\ell m}(\hat{\mathbf{n}})$ for the angular components, and spherical Bessel functions for the radial coordinate $j_\ell(k\chi)$; together, these functions constitute the spherical Fourier-Bessel basis. The shear tensor $\gamma(\chi, \hat{\mathbf{n}})$ is defined as the second $\eth$ derivative of the lensing potential Ψ

$$\gamma(\chi, \hat{\mathbf{n}}) = \frac{1}{2} \eth\eth\Psi(\chi, \hat{\mathbf{n}}). \qquad (35.8)$$

The shear γ can be expanded in the spherical Fourier-Bessel basis as

$$\gamma(\chi, \hat{\mathbf{n}}) = \sqrt{\frac{2}{\pi}} \sum_{\ell m} \int k^2 \, dk \, \gamma_{\ell m}(k) \, {}_2Y_{\ell m}(\hat{\mathbf{n}}) \, j_\ell(k\chi), \qquad (35.9)$$

where the coefficients $\gamma_{\ell m}(k)$ are given by

$$\gamma_{\ell m}(k) = \sqrt{\frac{2}{\pi}} \int \chi^2 d\chi \int d\Omega \, \gamma(\chi, \hat{\mathbf{n}}) \, j_\ell(k\chi) \, {}_2Y^*_{\ell m}(\hat{\mathbf{n}}). \qquad (35.10)$$

The covariance of shear modes can be related to the matter power spectrum [2164, 2178, 2179],

$$\langle \bar{\gamma}_{lm}(k) \bar{\gamma}^*_{\ell' m'}(k') \rangle = \frac{9\Omega_m^2}{16\pi^4 \chi_H^4} \frac{(\ell+2)!}{(\ell-2)!} \int \frac{d\tilde{k}}{\tilde{k}^2} \, G_\ell(k, \tilde{k}) \, G_\ell(k', \tilde{k}) \, \delta^K_{\ell\ell'} \, \delta^K_{mm'}.$$

where

$$G_\ell(k, k') = \int dz \, n_z(z) \, F_\ell(z, k) \, U_\ell(z, k'), \qquad (35.11)$$

$$F_\ell(z, k) = \int dz_p \, p(z_p|z) \, j_\ell[k\chi^0(z_p)], \qquad (35.12)$$

$$U_\ell(z, k) = \frac{1}{2} \int_0^{\chi(z)} \frac{d\chi'}{a(\chi')} \left(\frac{\chi - \chi'}{\chi\chi'}\right) j_\ell(k\chi') \, P_\delta^{1/2}(k, z(\chi)) \, \mu(k, a(\chi)) \left[1 + \frac{1}{\eta(k, a(\chi'))}\right]. \qquad (35.13)$$

The estimates $\bar{\gamma}$ of the pure cosmic shear field γ keep into account observational effects such as the redshift distribution $n_z(z)$ of the lensed galaxies and the conditional probability $p(z_p|z)$ of estimating the redshift z_p given the true redshift z. More recently, 3D cosmic shear was used in [2164] to forecast modified gravity predictions, with a quantitative comparison with a tomographic analysis, whose results we recall below.

35.2 Current Data and Forecasts on Horndeski Gravity

The Horndeski Lagrangian [2180] is the most general scalar-tensor theory of gravity with a scalar degree of freedom in addition to the metric, that respects the following conditions: it is four-dimensional, Lorentz-invariant, local and has equations of motion with derivatives not higher than second order. The latter condition guarantees that the theory is safe from Ostrogradski instabilities [197]. We will consider only universal coupling between the metric and the matter fields (collectively described by Φ_m and contained in the matter Lagrangian $\mathcal{L}_m$), which are therefore uncoupled to the scalar field. The Horndeski action can be written as follows:

$$S[g_{\mu\nu},\Psi] = \int d^4x\sqrt{-g}\left[\sum_{i=2}^{5}\frac{1}{8\pi G_N}\mathcal{L}_i[g_{\mu\nu},\Psi] + \mathcal{L}_m[g_{\mu\nu},\Phi_M]\right], \tag{35.14}$$

$$\begin{aligned}
\mathcal{L}_2 &= G_2(\Psi,X),\\
\mathcal{L}_3 &= -G_3(\Psi,X)\Box\Psi,\\
\mathcal{L}_4 &= G_4(\Psi,X)R + G_{4X}(\Psi,X)\left[(\Box\Psi)^2 - \Psi_{;\mu\nu}\Psi^{;\mu\nu}\right],\\
\mathcal{L}_5 &= G_5(\Psi,X)G_{\mu\nu}\Psi^{;\mu\nu}\\
&\quad - \frac{1}{6}G_{5X}(\Psi,X)\left[(\Box\Psi)^3 + 2\Psi_{;\mu}{}^{\nu}\Psi_{;\nu}{}^{\alpha}\Psi_{;\alpha}{}^{\mu} - 3\Psi_{;\mu\nu}\Psi^{;\mu\nu}\Box\Psi\right].
\end{aligned}$$

The subscripts Ψ, X denote partial derivatives, e.g. $G_{iX} = \frac{\partial G_i}{\partial X}$. The choice of the arbitrary functions $G_i(\Psi,X)$ of the scalar field Ψ and its kinetic term $X = -\frac{1}{2}\partial_\mu\Psi\,\partial^\mu\Psi$ determines the specific gravity model considered within this class. Several known models of dark energy and modified gravity are contained within this class, such as quintessence, $f(R)$ and Galileon models.

The evolution of linear perturbations in Horndeski gravity can be fully described by four functions of (conformal) time τ only [217, 2181]:

i) α_K is the *kineticity* function, representing the kinetic energy of the scalar perturbations arising directly from the action;

ii) α_B is the *braiding* function, which describes mixing of the scalar field with the metric kinetic term;

iii) α_M is the *Planck mass run rate*, describing the rate of evolution of the effective Planck mass;

iv) α_T is the *tensor speed excess*, describing deviations of the propagation speed of gravitational waves from the speed of light. This function has recently been constrained to be very close to 0, its General Relativity value, by the detection of the binary neutron star merger GW170817 and the associated gamma ray burst GRB170817A [1177, 2182].

Constraints on these functions can be obtained from large-scale structure observations by choosing a time parametrization, such as the one that traces the evolution of the dark energy component $\Omega_{\rm DE}(\tau)$:

$$\alpha_i(\tau) = \hat{\alpha}_i\Omega_{\rm DE}(\tau) \quad i = K, B, M, T \tag{35.15}$$

and getting constraints on the proportionality coefficients $\hat{\alpha}_i$. All of these functions are identically vanishing in General Relativity, so that any detection of a value different from 0 would be a clear signal of deviations from Einstein's gravity. This is the idea developed in [2164] and [2183], using cosmic shear as the cosmological probe (alone and in cross-correlation with other observables) to constrain Horndeski gravity.

In [2164], the authors present a Fisher matrix forecast for the Euclid survey, with the goal of quantitatively predicting its constraining power on Horndeski parameters as introduced above Eq. 35.2. The parameterization chosen for the evolution of the α functions is the one described by Eq. 35.15. The authors fix the values of α_K and α_T to 0, the former being largely uncorrelated with the other three functions and unconstrained by large-scale structure probes, the latter being strongly constrained by gravitational wave experiments. Moreover, they present a forecast comparing tomography and 3d cosmic shear, presenting expressions for both formalisms in a general modified gravity setting (similarly to the description provided in Sec. 35.1). They simultaneously place constraints on a set of cosmological parameters describing the evolution of the background (assumed to be well modelled by a ΛCDM model), as well as on the Horndeski parameters α_M and α_B, which act at the perturbation level. They find that a 3D analysis can constrain Horndeski theories better than a tomographic one, with a reduction of the errors of the order of 20% on the Horndeski parameters.

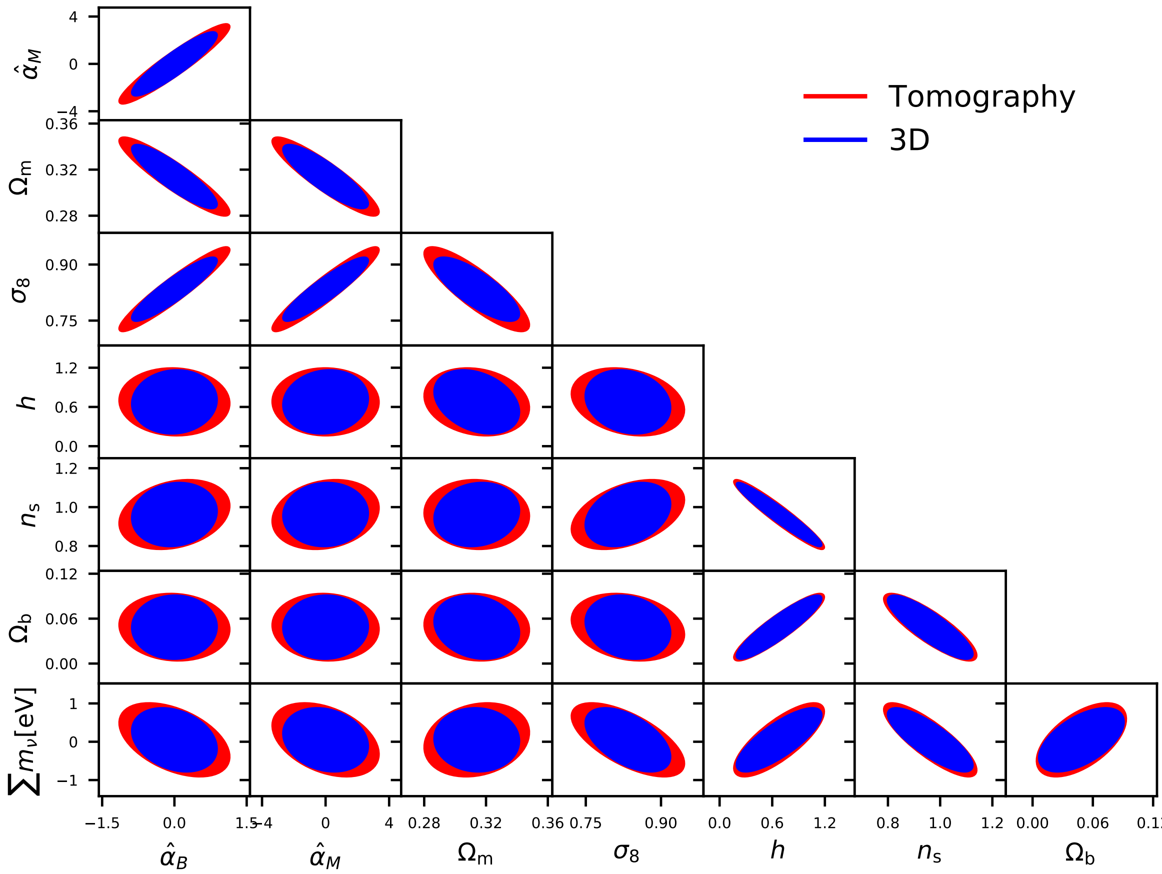

Figure 35.1: *1-σ Fisher forecast contours for Euclid-like survey, obtained with tomography (red) and 3D cosmic shear (blue). The parameters constrained are a set of standard cosmological parameters describing the evolution of the background and the Horndeski $\hat{\alpha}_B$ and $\hat{\alpha}_M$ parameters acting on the perturbations. As discussed in [2164], a 3D analysis tightens constraints on all standard and Horndeski parameters of about* 20% *with respect to a tomographic analysis. The figure is taken from [2164].*

Despite performing a conservative cut in angular and radial scales and only using a linear matter power spectrum for the calculation of the covariance of the cosmic shear modes, 3D cosmic shear performs better than tomography in constraining both standard and Horndeski parameters (as shown in Fig. 35.1, taken from [2164]). The two methods show similar degeneracies, despite being completely independent in their implementation and based on two different formalisms. To illustrate the importance of non-linear corrections, the authors produce constraints with 3D cosmic shear and a prescription for the non-linear matter power spectrum based on [2184]; the resulting increase in sensitivity from the non-linear corrections calls for the development of nonlinear prescriptions for general dark energy models in view of applications to future datasets.

In [2183], the authors present a cross-correlation analysis of cosmic shear, galaxy-galaxy lensing and galaxy clustering tomographic power spectra from $\sim$450 deg^2 of cosmic shear data from the Kilo Degree Survey (KiDS) and two overlapping spectroscopic samples from the GAlaxy and Mass Assembly (GAMA) survey. The goal of this analysis is to provide the first constraints on Honrdeski parameters achieved from currently available cosmic shear data (alone and in cross-correlation with the other two probes). The methodology followed to model the power spectra extends to a Horndeski gravity setting the analysis performed in [2185], carried out in ΛCDM on the same power spectra dataset. The authors adopt the same parameterization for the Horndeski α_B, α_M functions chosen in [2164] (and given by Eq. 35.15), finding values for $\hat{\alpha}_B$ and $\hat{\alpha}_M$ compatible with ΛCDM. Interestingly, the values found for $S_8 \equiv \sigma_8\sqrt{\Omega_m/0.3}$ (a combination of the parameters Ω_m and σ_8 particularly well probed by lensing) are in better agreement with the Planck CMB values when the analysis is carried out in Horndeski gravity, rather than in ΛCDM; the tension in the $\Omega_m - \sigma_8$ plane between large-scale structure and CMB measurements is largely reduced in Horndeski gravity (see Fig. 35.2).

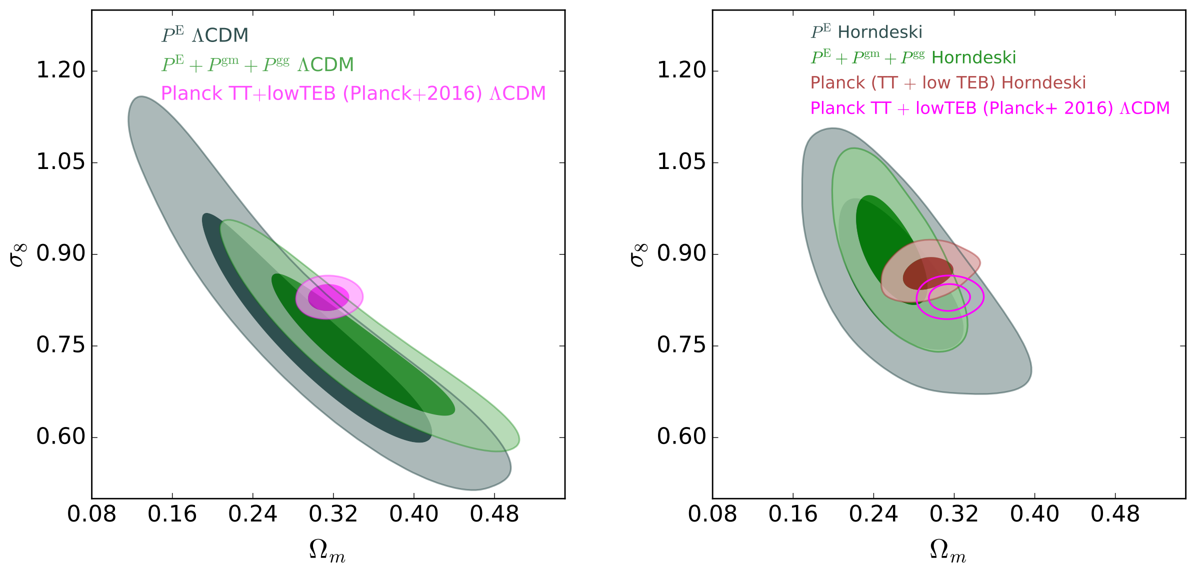

Figure 35.2: *68% and 95% contours on the cosmological parameters $\Omega_{\rm m}$ and σ_8. The grey contours are obtained considering $\sim$450 deg^2 of cosmic shear data from the KiDS survey; the green contours are obtained from a joint analysis of cosmic shear - galaxy-galaxy lensing and galaxy clustering from the same KiDS samples and two overlapping spectroscopic samples from the GAMA survey. In the left panel, large-scale structure and CMB probes are analysed assuming a ΛCDM model (the Planck contours in magenta are the same as in [2186]). In the right panel, the large-scale structure constraints are obtained assuming Horndeski gravity; in brown we plot the Planck contours assuming Horndeski gravity, whereas in magenta the ΛCDM contours of [2186] (the same as in the left panel) are reproduced for comparison.*

35.3 Higher-order Statistics and Lensing Peak Counts

Using different statistics, beyond the second-order Gaussian power spectrum, can help to capture non Gaussian content and better discriminate among different cosmological models. An analysis of a variety of different statistics in weak lensing observables has been extensively presented in [2163]. In particular, it is relevant to ask the following questions: if a non-standard gravity cosmology is mimicking a cosmological constant, can we distinguish the two scenarios using weak lensing? Which statistic best discriminates them? Massive neutrinos are degenerate with the strength of a fifth force gravitational interaction: higher values of the neutrino mass suppress the growth of structure, and can therefore compensate higher values of the strength of the fifth force interaction, which would enhance the growth. For example, an $f(R)$ model with amplitude $f_{R0} \sim 10^{-5}$ and massive neutrinos of $m_\nu \sim 1.5$eV can mimic the matter power spectrum of a cosmological constant model with a neutrino mass of 0.06 eV (as currently typically fixed in ΛCDM). Authors in [2163] then used hydro simulations for ΛCDM and different $f(R)$ cosmologies (of the type Hu-Sawicki), built on purpose to be degenerate in their matter power spectra. They then compared different statistics in weak lensing observables, including variance, skewness, kurtosis and peak counts, i.e. the number count of lensing peaks in their aperture mass maps.

Results show that peak counts best capture non-Gaussian information and represent the statistic that has a higher chance to discriminate between $f(R)$ and ΛCDM models, with a discrimination efficiency that depends on redshift and angular scale of observation. Figure 35.3 from [2163] nicely shows this effect for a specific filtering scale.

Peak counts are therefore a promising tool for future weak lensing surveys. In addition, as shown in forecasts presented in [2187], combining peak counts with lensing power spectrum can improve the constraints on the sum of neutrino masses, on the relative matter density Ω_m, and on the primordial amplitude A_s by factors 39%, 32%, and 60% respectively, as compared to constraints derived from the power spectrum alone [2188]. More recently, in [2189] the authors proposed a new statistics that joins peaks and voids, and avoids the problem of defining what is a peak or what is a void.

35.4 Machine Learning and the Dark Universe

Machine learning has recently seen an increase in applications in all fields, including cosmology for which new opportunities and challenges have been recently summarised in [1605]. Convolutional Neural Networks (CNN) have been used in particular on weak lensing observables, trained on convergence maps, to discriminate models along the Ω_m, σ_8 degeneracy [2190–2192]. In [2193] the authors also showed that the network can exploit information related to the steepness of local peaks, rather than to their amplitude. More recently, it was shown in [2194] that CNN can break the degeneracy discussed above between neutrino masses and the dark universe, significantly outperforming all statistics, including peak counts.

We briefly recall here the main result developed in [2194], as this directly compares with what discussed in 35.3 and the python code used in the analysis has been made publicly available: specifically, authors apply CNN to discriminating between ΛCDM cosmologies and $f(R)$ (Hu-Sawicki) models with massive neutrinos. The authors start from one simulation per model: this is possible for a classification problem, for which simulations are done on purpose for models which are degenerate at the level of the power spectrum. Convergence maps are then obtained with random reorientation in the same simulation run; furthermore, a compressed representation of the input is used, which reduces the dimentionality of the data and speeds up the training. As known, the network learning procedure consists in updating the parameters (weights) in the cost function via gradient descent and back-propagation in order to match the desired output.

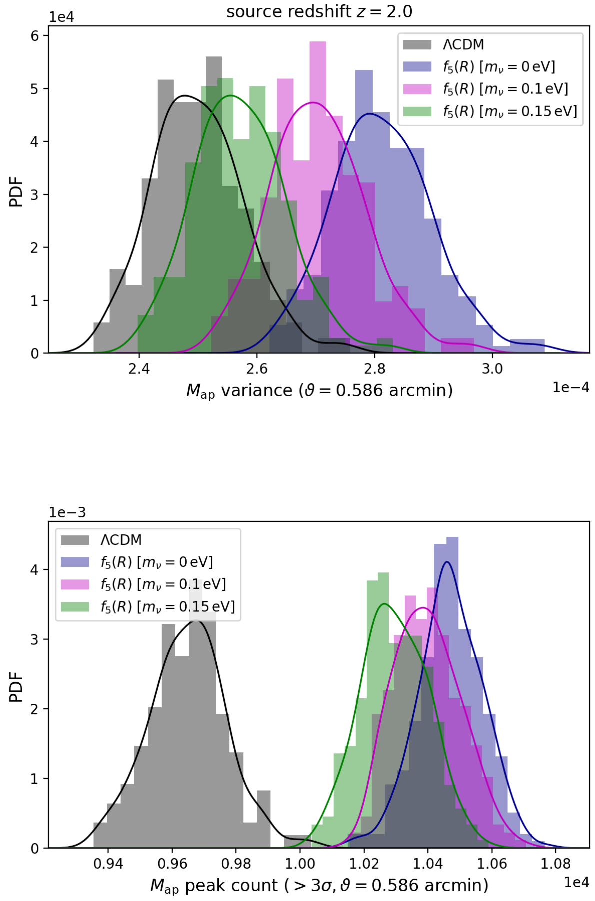

Figure 35.3: *Histograms of aperture mass statistics for ΛCDM and $f_5(R)$ models (i.e. Hu-Sawicki models with amplitude $f_{R0} = 10^{-5}$) and different values of the neutrino mass m_ν. Each histogram, with area normalised to one, comprises 256 samples of the statistic computed at a filtering scale of $\vartheta = 0.586'$ and for sources at redshift $z_s = 2.0$. Solid lines represent the result of smoothing the distribution by KDE (cf. Sect. 5.3 in [2163]). Considering the most degenerate case with ΛCDM, $f_5(R)$ with $m_\nu = 0.15$ eV, second- and higher-order moments of $M_{\rm ap}$ do not appear able to distinguish the models. Peak counts, on the other hand, shown here for a 3σ threshold, cleanly separate the two distributions. It is interesting to note that peak counts separate all $f_5(R)$ cases from ΛCDM by approximately the same amount, independent of m_ν. The figure is taken from [2163].*

This learning (training) process is done on 75% of the available input data (for which labels are known) and tested on the remaining 25% of input data. Validation accuracy (i.e. the ratio of correct predictions to the total number of test observations) has been shown to go from 92% (for a noiseless case) down to 48% for a pessimistic noise level.

The results in [2194] show that the CNN is able to discriminate ΛCDM from $f(R)$ gravity better than other statistics, including peak counts, for all choices of noise levels. For example, for an intermediate/optimistic noise level ($\sigma = 0.35$ standard deviation in Gaussian random noise), ΛCDM can be discriminated with 79% accuracy (against 30% maximum accuracy for peak count statistic, for the same redshift). Including all four source redshifts available $\{0.5, 1, 1.5, 2\}$ further increases CNN accuracy to 87% for the same noise level. With respect to peak count statistic, CNN also seems to be more efficient in discriminating among different neutrino masses, within

$f(R)$ scenarios. Different types of machine learning techniques were also tested on the same simulations in [2195], finding that CNN is the one that best performs, among the ones tested.

While the results are promising for classification problems, this proof of concept opens the path to new challenges. First, one may want to also address a regression problem, i.e. infer cosmological parameters from real data: in this case, one can expect many more simulations to be needed, and a different architecture to serve for regression. Second, one may expect weak lensing systematics to also play a role when dealing with real data, and it is not clear at this stage if machine learning will be robust to these systematics. This has to be investigated in the future.